

---

# New Methods for Numerical Simulation of Welding of Large Thin Structures

**Frédéric Faure\*\*\* — Jean-Michel Bergheau\*\*\*  
Jean-Baptiste Leblond\* — Bruno Souloumiac\*\***

\* LMM, UMR 7607 CNRS/Université Paris VI, Paris, France

\*\* ESI Software, Lyon, France

\*\*\* LTDS, UMR 5513 CNRS/ECL/ENISE, Saint-Etienne, France

---

*ABSTRACT. Welding of thin structures often leads to distortions that must be controlled. Whereas numerical simulation of small structures is relatively easy, severe difficulties are encountered in the simulation of large ones. Indeed the mesh must be considerably refined in the heat affected zone, and this leads to huge simulations and prohibitive computation times. Three alternative methods are presented here to circumvent this problem. The first one consists of using only shell elements. The second method consists of using shell elements far from the heat source and a mobile local 3D mesh close to it. The third method is a "local/global" approach which consists of first performing a local 3D simulation of a short portion of the welding bead, and then introducing inelastic strains into some global shell simulation of the full structure. These methods are critically assessed by comparing their results to those of a full 3D simulation in the typical case of a welded plate.*

*RÉSUMÉ. Le soudage de structures minces provoque des distorsions qui doivent être contrôlées. Mais, alors que la simulation numérique du soudage sur de petites structures est aujourd'hui assez bien maîtrisée, la simulation de grandes structures se heurte à d'importantes difficultés. En effet, la nécessité de raffiner le maillage dans la zone affectée thermiquement le long des joints soudés conduit à des simulations énormes, beaucoup trop coûteuses en temps de calcul. Cet article présente trois méthodes pour résoudre ce problème. La première n'utilise que des éléments coques. La seconde met en œuvre un maillage 3D massif mobile le long du joint soudé et des éléments coques ailleurs. La troisième, dite "locale/globale" consiste à réaliser un calcul local 3D sur une petite portion du joint puis à transférer les déformations inélastiques sur le maillage coque de la structure complète. Ces méthodes sont évaluées en comparant leurs résultats avec ceux obtenus par une analyse transitoire sur un maillage ne comportant que des éléments massifs 3D, dans le cas typique d'une plaque soudée.*

*KEYWORDS: welding, finite element, shell element, adaptive refinement, local/global approach.*

*MOTS-CLÉS: soudage, éléments finis, élément coque, maillage adaptatif, approche locale/globale.*

---

## 1. Introduction

Welding is the main joining technique used in industry. However, welding processes lead to residual stresses and distortions that must be controlled. Experiments provide irreplaceable, but partial informations about these stresses and distortions, and the only way to fully know them is to perform finite element simulations accounting for the complex interactions between thermal, metallurgical and mechanical phenomena.

2D or 3D local meshes give satisfactory stress predictions in the heat-affected zone (HAZ). However, in the case of large and thin structures like coachworks, important distortions are generated even far from the HAZ. The prediction of these distortions raises severe difficulties. Indeed, whereas a fine, often fully 3D mesh is necessary in the HAZ because of large variations of thermal, metallurgical and mechanical fields in this zone, a complete mesh of the whole structure is compulsory to evaluate remote distortions; but a complete 3D mesh is ruled out because of heaviness and cost of the calculation.

In order to avoid such heavy computations, different methods have been developed. The most popular one consists of mixing 3D and shell elements. However, in its simplest version, this method requires the use of a fine 3D mesh for the entire welding bead (Gu and Goldak, 1991)(Nasstrom *et al.*, 1991). Three alternative approaches are presented in this paper.

The first one consists of using only shell elements (*shell approach*). Lindgren (2002) has showed that this is possible even in the HAZ in specific cases. In the present work, the thermal computation is based on the assumption of a quadratic through-the thickness variation of temperature. The metallurgical calculation is fully coupled with the thermal one and based on a multi-layer approach. The mechanical computation, which duly accounts for the effect of phase changes and notably transformation plasticity, is also based on a multi-layer scheme. The performances of the new “welding shell element” thus defined are assessed by comparing the results of some simulation using it with those of a 2D axisymmetric simulation, in the simple case of a disk subjected to some thermal cycle through illumination of one of its faces by a laser beam. The results of both simulations are also compared to experimental measurements.

The second method consists of mixing 3D and shell elements, use of 3D elements being restricted to a small block around the HAZ (*adaptive 3D/shell approach*). In contrast to the classical 3D/shell method which involves meshing of the complete welding bead with solid elements, this local 3D mesh represents only a small portion of the bead, which implies that it must move with the heat source within the coarser shell mesh. Because of this motion, thermal, metallurgical and mechanical quantities must be “transferred” from shell to 3D elements ahead of the source and from 3D to shell elements behind it.

The last method is a *local/global approach*. It consists of 2 steps. The first one (local step) consists of performing a transient analysis of a short portion of the welding bead and HAZ using a 3D mesh. The boundary of this small zone is assumed to be traction-free in the mechanical simulation; the assumption made here is that plastic strains essentially depend on local thermal and mechanical fields and are little affected by the clamping effect arising from the stiffness of the rest of the structure. The output of this step consists of local inelastic residual strains due to welding. The second one (global step) consists of performing an elastic simulation of the full structure using shell elements; the inelastic strains determined previously are then introduced in some “macro-elements” which represent the welding bead and the HAZ. This step provides far distortions of the whole structure after complete cooling and unclamping.

The validity of these 3 approaches is finally assessed by performing numerical simulations of welding of a thin plate, and comparing the results obtained using each of them to those of some fully 3D “reference” simulation.

## 2. Welding shell element

### 2.1. Generalities

In the first method proposed, shell elements are used even in the HAZ. Thus they should incorporate special constitutive laws accounting for phenomena occurring during phase changes and notably transformation plasticity. Previous welding simulations which used shell elements even in the HAZ (Dong *et al.*, 1997) (Lindgren and Karlsson, 1988) disregarded effects arising from phase changes.

The constitutive laws used here account for such effects in all steps of the simulation: thermal, metallurgical and mechanical. The thermal analysis accounts for dependence of thermal properties upon temperature and metallurgical phases, and also for transformation latent heats; thus the thermal and metallurgical calculations are necessarily coupled and performed simultaneously, although they are presented separately below for the sake of clarity. The metallurgical and mechanical calculations are based on a multi-layer formulation similar to that commonly used for composite shells. The mechanical computation accounts for transformation plasticity and also various, notably geometrical, nonlinearities.

### 2.2. Thermal computation

The heat conduction equation in the shell reads:

$$\operatorname{div}\left(\lambda \overline{\operatorname{grad} \theta}\right) - \rho \frac{\partial H}{\partial t} = 0 \quad [1]$$

where  $\theta$  denotes the temperature and  $\lambda, \rho, H$  the thermal conductivity, mass per unit volume and enthalpy per unit mass, all 3 of which depend on  $\theta$  and the proportions of the phases. This equation is used in this form without expressing  $\partial H / \partial t$  as  $c \partial \theta / \partial t$  where  $c$  denotes the apparent specific heat; an enthalpic formulation fully coupled with calculation of phase changes (involving calculation of  $H$  as a function of  $\theta$  and the proportions of the phases at each time step) is used instead. Such a formulation is well fit to problems involving phase changes occurring within a narrow range of temperature, and also allows to account for different transformation kinetics upon heating and cooling in a rigorous way, without “cheating” through introduction of different apparent specific heats during these 2 periods. Also, nonlinear boundary conditions accounting for thermal losses due to convection and radiation are used on the upper and lower faces of the shell.

Since the shell is assumed to be thin, one can assume some simple through-the-thickness temperature profile (Voldoire and Andrieux, 1993). This profile is generally assumed to be polynomial (Surana and Abusaleh, 1990), but other strategies are possible. The simplest assumption of a linear profile has been used in (Rubin, 1986), but such a profile imposes an often undesired restriction, namely equal input and output heat fluxes on the faces of the shell. Another approach (Surana and Phillips, 1987) consists of defining some “finite element degenerated” thermal shell element through condensation of the degrees of freedom (d.o.f.) of some 3D element in the direction of the thickness. The formulation adopted here is based on the assumption of a quadratic through-the-thickness variation of temperature. The temperature at any point  $Q$  of the shell volume at time  $t$  is thus given by:

$$\theta(Q, t) = \theta_m(P, t) + \alpha(P, t)z + \beta(P, t)z^2 \quad [2]$$

where  $\theta_m(P, t)$  denotes the temperature at the projection  $P$  of point  $Q$  onto the mid-surface of the shell,  $z$  the distance from point  $P$  to point  $Q$ , and  $\alpha(P, t)$ ,  $\beta(P, t)$  coefficients. These coefficients are readily determined in terms of  $\theta_m(P, t)$  using boundary conditions on the faces of the shell. Thus there is a single nodal d.o.f.,  $\theta_m(P, t)$ .

### 2.3. Metallurgical computation

There are two types of solid-state transformations in steels:

- diffusional transformations (for instance ferritic and austenitic transformations), isothermal kinetics of which are usually described through Johnson-Mehl-Avrami type laws;

– martensitic transformations; the volume fraction of martensite depends only on temperature (the lesser influence of stresses being disregarded) and is usually assumed to be given by Koistinen-Marburger’s formula.

The anisothermal kinetics of both types of transformations are described here using a single heuristic model due to Leblond and Devaux (1984). In the simple case of 2 phases only,  $\alpha$  and  $\gamma$ , with volume fractions  $p_\alpha$  and  $p_\gamma = 1 - p_\alpha$ , and a transformation from phase  $\gamma$  to phase  $\alpha$ , the evolution equation for  $p_\alpha$  reads:

$$\dot{p}_\alpha = \frac{p_{\alpha eq}(\theta) - p_\alpha}{\tau_{\gamma \rightarrow \alpha}(\theta)} \quad [3]$$

where  $p_{\alpha eq}(\theta)$  denotes the “equilibrium” proportion of phase  $\alpha$  at temperature  $\theta$  and  $\tau_{\gamma \rightarrow \alpha}(\theta)$  some characteristic reaction time.

#### 2.4. Multi-layer “thermo-metallurgical” shell element

Whereas the through-the-thickness *temperature* profile is assumed to depend on 3 coefficients only, such an approximation is impossible for the *metallurgical* calculation due to the usually sharp variations of the proportions of the phases within the thickness. A multi-layer approach, similar to that commonly used for composite shells, is therefore adopted for calculation and storage of the proportions of the phases.

#### 2.5. Mechanical shell element

Mechanical shell elements available in the literature fall into 2 categories according to whether they are based on some Kirchhoff-Love-type or Mindlin-Reissner-type theory. Elements of the first type are seldom used, first because they do not apply to thick shells, second because they require interpolations of class  $C^1$  which raise considerable numerical difficulties. Mindlin-Reissner-type elements are easier to handle and more commonly used, although they also raise such difficulties as discontinuities of the tangent plane between adjacent elements and transverse shear locking. In this work, we adopt the Mindlin-Reissner-type “T1-element” of Hughes and Tezduyar (1981). Although quite old, this simple element is “battle-tested” and applies to thin as well as thick shells. It was originally developed within a linearized context but the version used duly accounts for large displacements, as needed for accurate prediction of welding residual distortions.

### 2.6. Mechanical model for transformation plasticity

Solid-state transformations occurring during cooling of steels induce some anomalous plastic behaviour termed “transformation plasticity”. Two physical explanations have been proposed for this phenomenon. Greenwood and Johnson (1965) ascribe transformation plasticity to micro-plasticity in the weaker  $\gamma$  phase arising from the difference of specific volume between the phases. Magee (1966) ascribes transformation plasticity (during martensitic transformations only) to formation of martensite plates with some preferred orientation depending on the load applied. The model used here is due to Leblond *et al.* (1989). Although it considers only Greenwood-Johnson’s mechanism, it gives good results for most steels. In this model, the “transformation plastic strain rate” ( $\dot{\epsilon}_{ij}^{tp}$ ) which must be added to the classical plastic strain rate is of the form (assuming strain hardening to be of isotropic type for simplicity):

$$\dot{\epsilon}_{ij}^{tp} = -\frac{\Delta V/V}{\sigma_{\gamma}^Y} s_{ij} \left( \ln p_{\alpha} \right) \dot{p}_{\alpha} \quad [4]$$

(for a  $\gamma \rightarrow \alpha$  transformation, as occurs during cooling). In this expression  $\Delta V/V$  denotes the relative difference of specific volume between the phases,  $\sigma_{\gamma}^Y$  the yield stress of austenite and ( $s_{ij}$ ) the stress deviator.

Just like for the metallurgical calculation, a multi-layer approach is used for the mechanical calculation because of the sharp variations of the stresses and plastic strains within the thickness. Membrane and bending generalized strains are thus converted into usual 3D strains in each layer using the Mindlin-Reissner kinematic assumption; a “plastic correction” based on equation [4] is then applied to the “elastically calculated” 3D stresses; finally integration of these corrected 3D stresses over the thickness yields membrane and bending generalized stresses.

### 3. Assessment of the welding shell element

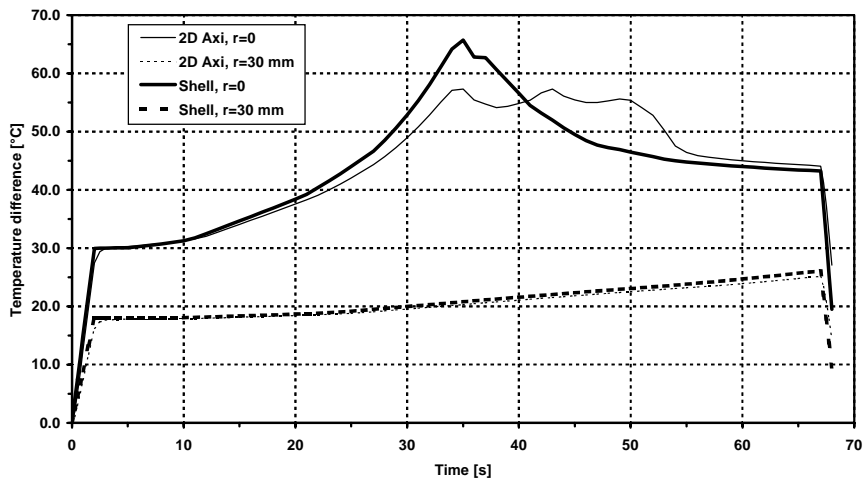
The first task is to critically assess the performances of the newly developed “welding shell element”. This will be done by comparing the results of some simulation using it with those of a standard 2D axisymmetric simulation and also with experimental results, in the case of a heated disk.

The experimental procedure is described in detail in (Vincent, 2002) and (Bergheau *et al.* 2004). The disk, of radius 160 mm and thickness 5 mm, is made of 16MND5 steel (French norm; this is equivalent to A508 in the American norm). The thermal, metallurgical and mechanical properties of this steel are provided in

(ASTM, 1991) (Waeckel, 1994). The upper face of the disk is illuminated by a CO<sub>2</sub> laser beam. The heat input is chosen in such a way that the central part of the disk reaches an austenitic state during heating without melting; this eliminates poorly known phenomena like convection in the molten pool, which are of course present in actual welding experiments but would hamper here “neat” comparison of experimental and numerical results. The quantities measured include temperature, residual stresses (determined through X-ray diffraction) and final deformed shape of the disk.

The welding shell element has been implemented in, and the calculations performed with, the commercial finite element code SYSWELD® (2002).

In the thermal simulation, the value of the heat flux absorbed by the upper face has been determined by an inverse method so as to correctly reproduce the measured temperature. The values of the convective and radiative heat transfer coefficients governing losses are  $H_c = 15 \text{ W/(m}^2\text{°C)}$  and  $H_r(T) = \varepsilon\sigma(T^2 + T_{ext}^2)(T + T_{ext})$  where  $T$  denotes absolute temperature,  $\sigma$  (Stefan’s constant) =  $5.67 \cdot 10^{-8} \text{ W/(m}^2 \text{K}^4)$  and  $\varepsilon$  (thermal emissivity) = 0.75. These transfer coefficients are artificially slightly increased on the lower face in order to account for the extra cooling effect due to the support.



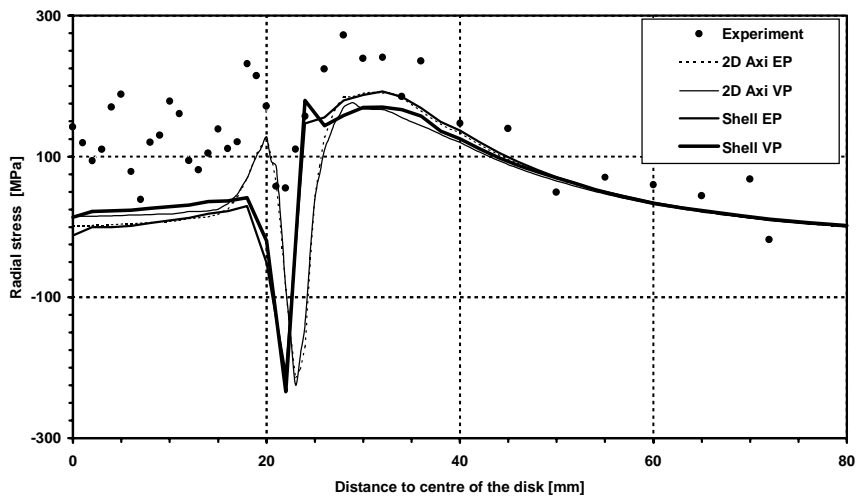
**Figure 1.** Temperature difference between the faces of the disk

Figure 1 shows the difference of temperature between the faces of the disk at 2 positions as a function of time, for the 2 simulations. (Showing experimental results would be pointless since the heat flux density used in the simulations was adjusted so

as to fit them). The agreement is quite acceptable, which shows that the assumption of a quadratic through-the-thickness variation of temperature used in the thermal shell element is reasonable. (This is because the geometry and heat input are both quite simple; other, less simple geometries and/or heat inputs can give rise to more complex distributions of temperature, as will be seen below).

The metallurgical simulation accounts for the austenitic transformation during heating as well as ferritic, bainitic and martensitic transformations during cooling. It also incorporates tempering effects which occur in that zone heated just below the  $AC_1$  temperature. (These effects are simulated by considering fictitious transformations from “as-quenched” structures to some “completely tempered” one). Computed results (not shown for space reasons) are in close agreement with experimental ones.

In the mechanical computation, all material properties are considered as temperature-dependent except for Poisson’s ratio. Dependence of thermal strain, yield limit and hardening slope upon the metallurgical phases is also accounted for, as well as transformation plasticity. Strain hardening is assumed to be of isotropic type. Two mechanical simulations are performed, with elastoplastic and elastoviscoplastic options respectively.



**Figure 2.** Radial stress as a function of distance from the centre of the disk

Figures 2 and 3 show the measured and computed radial and tangential stresses on the upper face of the disk, as functions of distance from its centre. Both options yield reasonable results. In spite of experimental errors, Figure 3 suggests that the elastoviscoplastic option is better; as explained in (Bergheau *et al.*, 2004) and

(Vincent *et al.*, 2003), this is because it duly accounts for the fact that the yield stress is lower during cooling than during heating since the strain rate is much lower (because the cooling rate is much lower than the heating rate), whereas the elastoplastic option does not. With regard to the comparison between the shell and 2D axisymmetric simulations, one observes that the agreement is quite good, except for the slight increase of the radial stress towards the edge of the HAZ, just before the big drop, which can be observed in the 2D axisymmetric calculation (in both options) but not in the shell simulation; see Figure 2. The probable explanation of this slight discrepancy is that the refinement of the mesh in this zone is insufficient in the shell simulation.

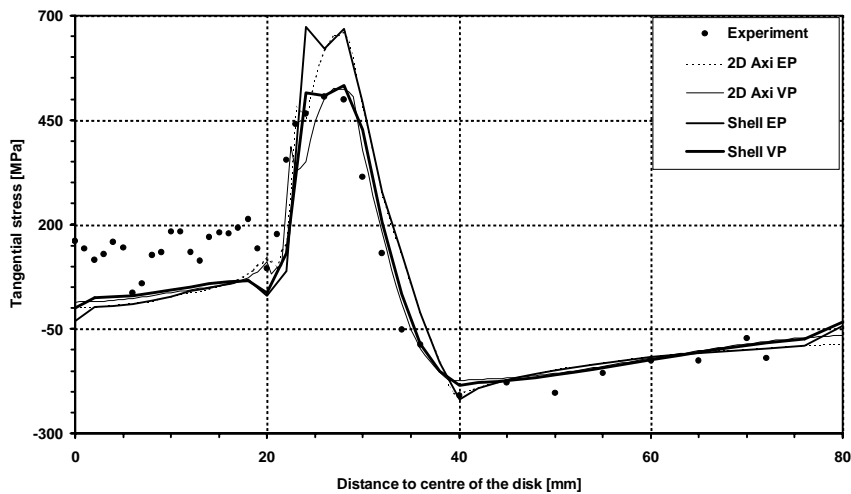


**Figure 3.** Tangential stress as a function of distance from the centre of the disk

Figure 4 shows the measured and computed axial displacements of the centre of the disk as a function of time. There is a large discrepancy here between results obtained with the elastoplastic and elastoviscoplastic options, those corresponding to the latter option being in much better agreement with experimental observations. This illustrates the fact (already mentioned in Bergheau *et al.*, 2004) that obtaining good calculated residual distortions is much harder than obtaining good residual stresses, because distortions are sensitive to tiny details of the material behaviour which have little influence on stresses. One also observes that the difference between results obtained with the 2D axisymmetric and shell simulations is small.

Finally Figure 5 compares axial displacements obtained (using shell elements and an elastoplastic option) by using a “small displacement” hypothesis and a “large displacement” one. Clearly, making a “small displacement” hypothesis results in considerable underestimation of the axial displacement. This is an indication that

distortions are primarily governed by geometrical nonlinearities arising from thermal buckling (due to large thermal expansion at high temperatures, and also during the  $\gamma \rightarrow \alpha$  transformation during cooling). This means that they are more sensitive to the *average value* of the temperature in the thickness of the disk than to its *gradient*, which explains, to some extent, why the simple assumption of a quadratic through-the-thickness temperature distribution suffices to obtain good distortions.

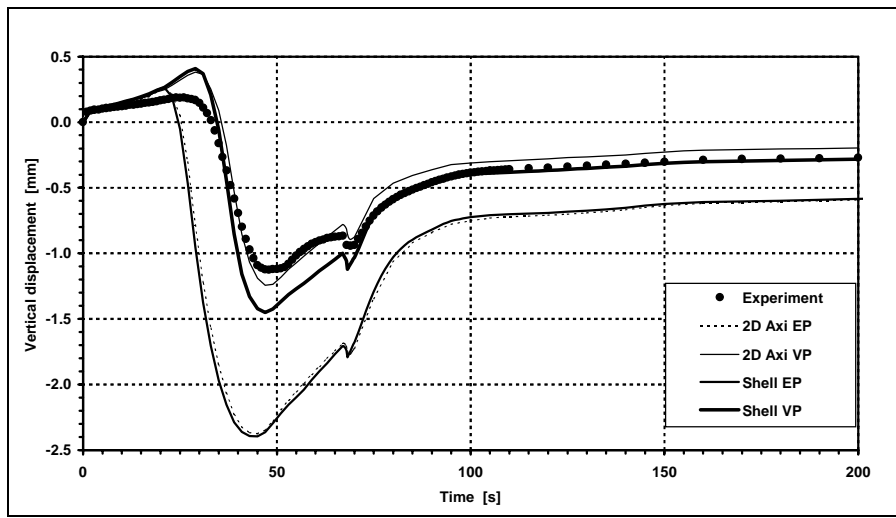


**Figure 4.** Vertical displacement of the centre of the disk

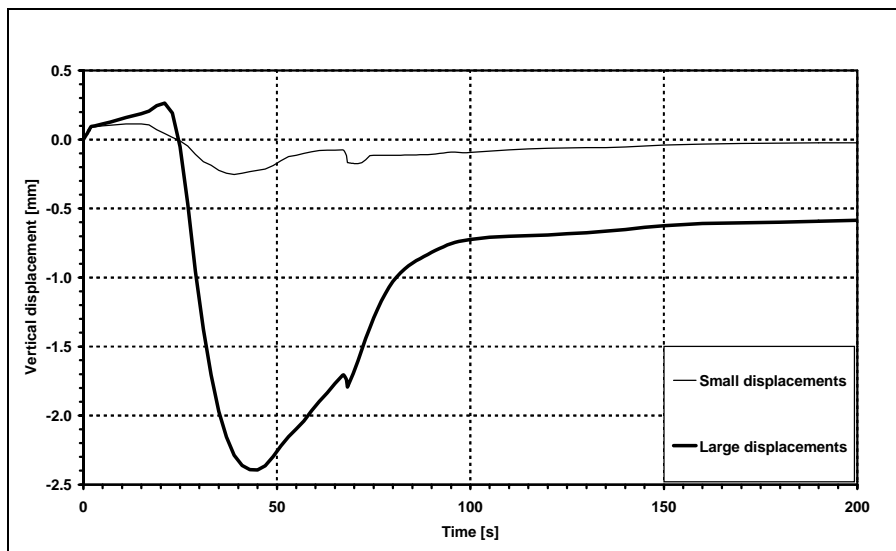


**Figure 5.** Comparison of vertical displacements obtained with “small displacement” and “large displacement” options

#### 4. Adaptive 3D/Shell approach

This method consists of mixing 3D and shell elements, use of 3D ones being restricted to a small portion of the welding bead so as minimize the number of d.o.f. This means that the block of solid elements must move with the source, which implies transfer of quantities from shell to solid elements ahead of the source and back from solid to shell elements behind it.

##### 4.1. Shell and 3D meshes

Most of the structure is meshed with shell elements, using the element described previously. This shell mesh must be regular but need not be very refined. The block of solid elements must begin just ahead of the heat source, and extend over a sufficient distance behind it and be wide enough to entirely contain the HAZ at the instant considered. The number of layers in the shell mesh governs the number of 3D elements in the thickness of the block, because we want the vertical positions of the nodes of the 3D elements to correspond to those of the layers. On the other hand, there is no necessary correspondence of shell and 3D meshes in the shell plane; in the example shown below, for instance, each shell element corresponds to 4 solid elements in this plane (Figure 6).

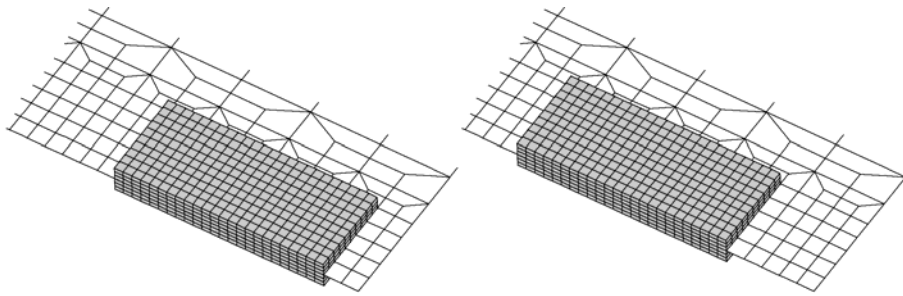


**Figure 6.** *Finite element mesh at successive instants*

##### 4.2. Generalities on transfer of values

Three types of transfer of quantities, corresponding to different zones, are required for both Gaussian and nodal values (Figure 7). In the first zone, ahead of the heat source, quantities must be transferred from shell to solid elements. In the second zone, they must be transferred from 3D to 3D elements; since the mesh is identical at successive instants in this zone, this operation only requires to correctly change the node and Gauss point numbers. In the third zone, behind the source, quantities must be transferred from 3D to shell elements.

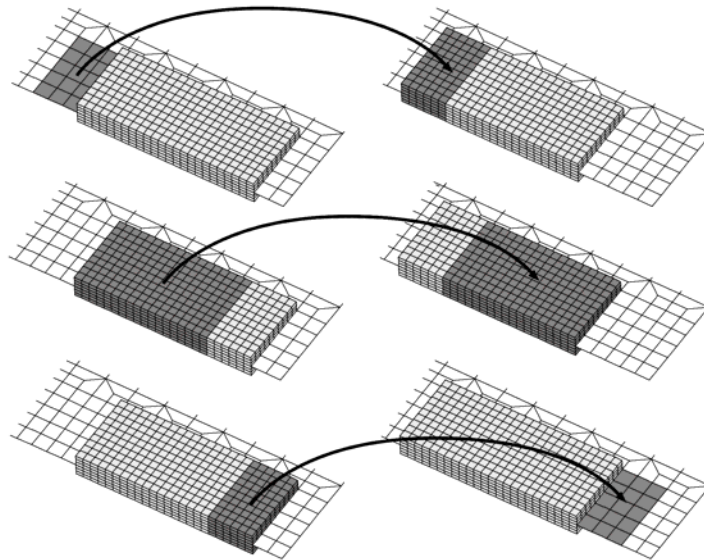


**Figure 7.** *The 3 types of transfer*

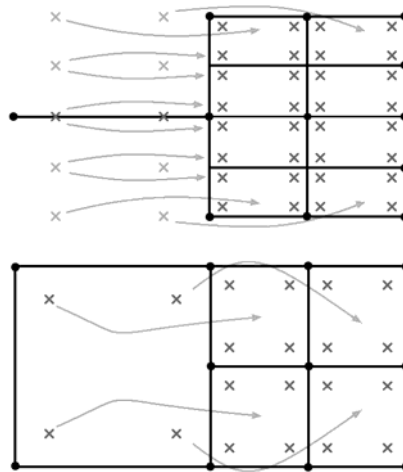


**Figure 8.** *Transfer of Gaussian values from shell to 3D elements*

### 4.3. *Transfer of Gaussian values*

In the first zone, values (of proportions of phases, plastic strains, etc.) at each Gauss point of the shell mesh are transferred to those Gauss points of the 3D block located nearest to it in the thickness direction (Figure 8, top). Also, since 4 solid elements correspond to one shell element in the shell plane, values at one Gauss point of the shell mesh are transferred to all 4 Gauss points of the 2 adjacent 3D elements (Figure 8, bottom).

In the third zone, opposite transfers are carried out. Values at the Gauss points of the 3D mesh are averaged out over the 4 points located at the same vertical position in each element, then over the 2 vertical positions adjacent to each layer, prior transfer to Gauss points of layers of the shell mesh.

Transfer of stress values implies slight violation of equilibrium just after transfer, but equilibrium is achieved again at the end of the iterative process of the next time-step.

### 4.4. *Transfer of nodal values*

In the thermal analysis, transfer of nodal values is simple because the number of d.o.f. is the same (1) for both meshes. For the transfer from shell to 3D nodes, shell nodal temperatures cannot be used because they are calculated only on the mid-surface of the shell. Therefore temperatures at the Gauss points of the shell mesh are used. More specifically, the temperature at each Gauss point of each layer of the shell mesh is transferred to the nearest 3D node; since there are 4 Gauss points in the shell mesh located at the same, minimal distance from each 3D node, the temperatures at these 4 Gauss points are averaged prior transfer to this node. Also, this defines nodal temperatures only at certain, “primary” 3D nodes; other nodal temperatures at “secondary” 3D nodes are then obtained through linear interpolation. For the inverse transfer, only temperatures on the mid-surface of the shell need be transferred; the operation is straightforward since each shell node corresponds to some 3D node.

In the mechanical analysis, the process is more complicated because there are 3 d.o.f. for each 3D node versus 6 for each shell node. For the transfer from shell to solid elements, the displacements of 3D nodes are deduced from displacements and rotations of shell nodes using the Mindlin-Reissner kinematic hypothesis. For the inverse transfer, the displacements of shell nodes are obtained by averaging the displacements of 3D nodes over the thickness. The rotation about the axis perpendicular to the welding direction is also deduced from the displacements of 3D nodes lying on the same normal to the shell plane, whereas the rotation about the welding direction is deduced from the displacements of 3D nodes lying on the mid-surface of the shell.

## 5. Local/Global approach

Theoretical features of the “local/global” approach have been expounded in detail in a previous paper (Souloumiac *et al.*, 2002) and will only be briefly recalled here. We consider only the simple case of deposition of a weld bead along the middle axis of a rectangular plate.

The first, “local” step consists of thermal, metallurgical and mechanical simulations performed on a “reduced” 3D geometry (Figure 9, left). In the mechanical simulation, the boundary of the zone considered is assumed to be traction-free. This means disregarding the “clamping effect” arising from the stiffness of the rest of the structure.

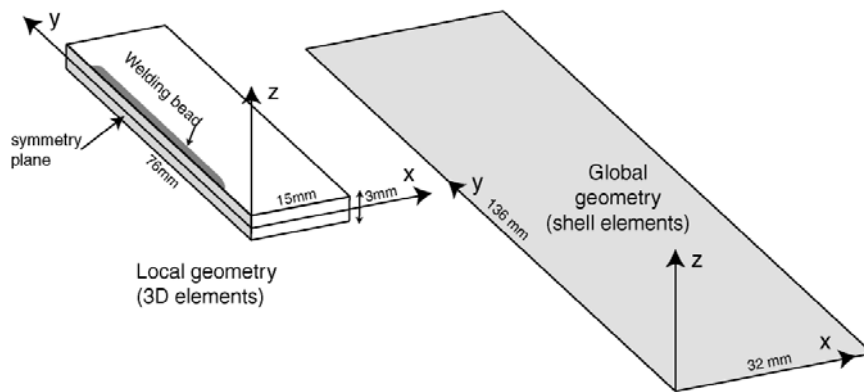


**Figure 9.** Local and global geometries

The residual plastic strain field obtained in the local simulation is prescribed as an “initial” strain in the global simulation (Figure 9, right) by means of *welding macro elements* (WME). WME have an effect in this simulation through their stiffness matrix and load vector, the calculation of which is sketched below.

In the present case, we use 3 types of WME, corresponding to 3 subdomains of the local geometry (Figure 10). The first and third subdomains include the start- and endpoints of the weld bead, corresponding to the beginning and end of the welding process, while the second one represents the central part of the bead, corresponding to the stationary stage of the process. They together include the entirety of the zone where plastic strains are nonzero.

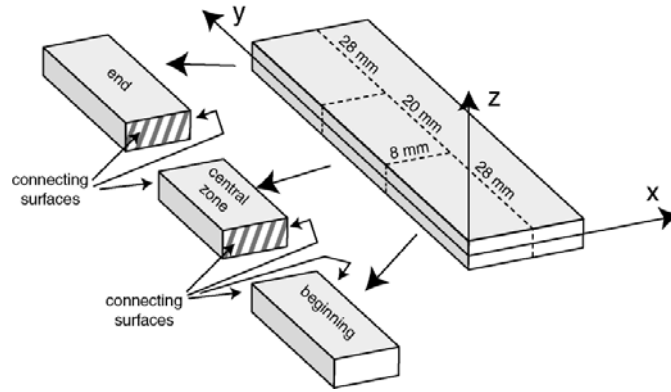


**Figure 10.** Extraction of subdomains from the weld bead zone

The stiffness matrix and load vector associated to each WME can be evaluated using the principle of virtual work in each subdomain  $\Omega$ . This principle reads, in the absence of an external loading :

$$\int_{\Omega} \varepsilon^* : \sigma \, dv = 0 \quad \text{with} \quad \sigma = E : (\varepsilon - \varepsilon^P)$$

Using the FE matrix formulation of the previous equation, one gets :

$$[K_{\Omega}] \{U\} = \{F_{\Omega}\} \quad [5]$$

where

$$[K_{\Omega}] = \sum_{\text{elements}} \int_{\Omega_e} [B_e]^T [E] [B_e] \, dv$$

is the stiffness matrix and

$$\{F_{\Omega}\} = \sum_{\text{elements}} \int_{\Omega_e} [B_e]^T [E] \{\varepsilon^P\} \, dv$$

the load vector resulting from the plastic strain field. These equations provide the stiffness matrix and load vector of the subdomain for the local 3D simulation. This matrix and vector must undergo 2 transformations prior to being used in the global shell simulation. The first one consists of condensing equation [5] onto the nodes of the outer boundary (“connecting surfaces”) of the subdomain through elimination of displacements of internal nodes (Figure 11, left). The second one consists of further

condensation onto WME nodes through elimination of displacements of nodes of connecting surfaces, the Reissner-Mindlin kinematic hypothesis being used to express these displacements in terms of the translation and rotation d.o.f. of the WME nodes (Figure 11, middle). The outputs of these transformations are the stiffness matrix  $[K_{WME}]$  and load vector  $\{F_{WME}\}$  of the WME.  $[K_{WME}]$  and  $\{F_{WME}\}$  are finally assembled with the stiffness matrix and load vector of other elements of the global mesh to get the overall stiffness matrix and load vector (Figure 11, right). Note that several (4 in Figure 11) WME of type 2, corresponding to the stationary stage of the welding process, can be assembled in the global simulation in order to represent long welding beads.

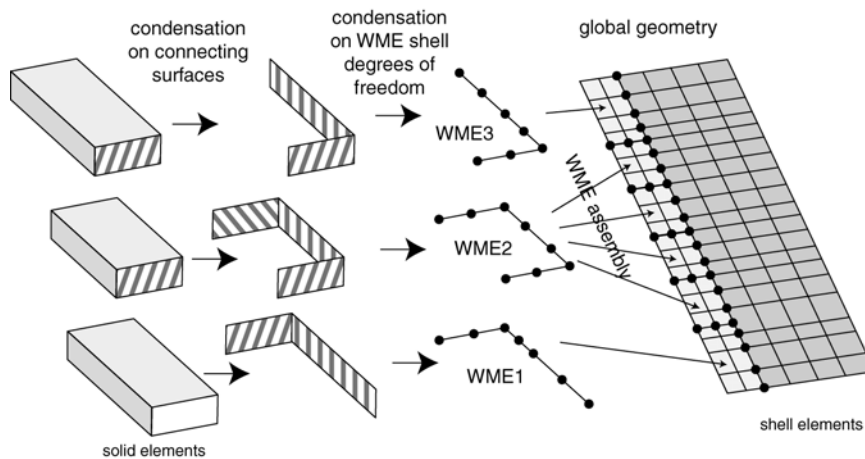


**Figure 11.** *Welding macro element calculation and assembly*

In the present stage of development of SYSWELD®, the updated Lagrangian algorithm used to account for geometrical nonlinearities in shells does not allow to include WME in the mesh. Thus simulations using WME must necessarily be performed with a small displacement hypothesis. Also, since elements other than WME are located far from the heat source, their behaviour is purely elastic. Thus only one resolution of the global system of equations is needed to get global distortions.

## 6. Numerical simulations

Simulations of welding of a thin plate have been performed to critically assess the different methods proposed, using a full 3D simulation as a reference. The plate

is a parallelepiped 136 mm long, 64 mm wide and 3 mm thick. The weld bead is 120 mm long. It is located on the middle axis of the plate so that only one half of the structure need be meshed. The material is 16MND5 steel as before. Again, the methods developed have been implemented in, and calculations performed with SYSWELD® (2002).

The full 3D mesh (Figure 12a) consists of 12963 nodes and 4424 quadratic subintegrated elements. (A calculation with linear elements has also been carried out). Even with such a large number of d.o.f., elements are quite large; their dimensions increase from  $1.7 \times 1.7 \times 0.75$  mm near the weld bead to  $5 \times 5 \times 1.5$  mm near the edge of the plate. Other 3D meshes, used in the adaptative 3D/shell and local/global approaches, are more refined near the weld, with typical dimensions  $1 \times 1 \times 0.5$  mm. The complete shell mesh (Figure 12b) consists of 1734 elements and 1826 nodes, and 7 layers are used to discretize the thickness. The 3D/shell mesh (Figure 12c) consists of 4802 3D and shell elements and 4565 nodes; the solid block is 44 mm long and 12 mm wide, and is displaced 8 times by 12 mm to simulate the motion of the heat source. The local geometry of the local/global approach (Figure 12d) consists of a parallelepiped with dimensions  $76 \times 15 \times 3$  mm discretized with 9576 elements and 8624 nodes. Once the mechanical calculation is over, this local geometry is divided into 3 subdomains 28 mm, 20 mm and 28 mm long, and only 8 mm wide because there is no plastic strain beyond. Each of these subdomains is “transformed” into some WME using the procedure sketched above. The second WME is duplicated 4 times to get the full portion of the bead corresponding to the stationary stage of the welding process. (This is why the length of the zone considered in the local simulation, 76 mm, is smaller than the actual length of the weld bead, 120 mm). The global mesh consists of 136 shell elements with dimensions  $4 \times 4.25$  mm.

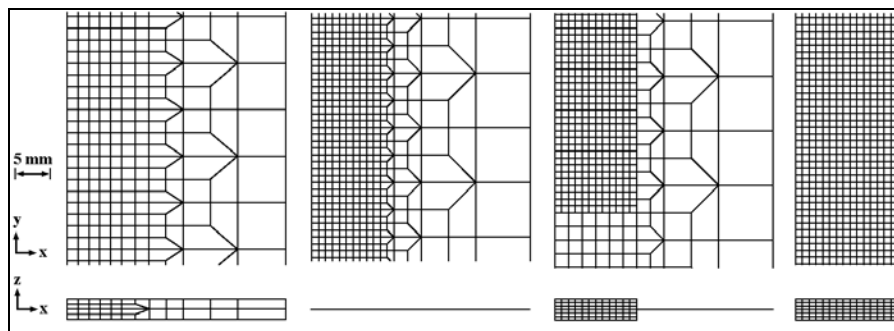


**Figure 12.** Finite element meshes : 3D, shell, 3D/shell, local mesh of local/global method

In the thermal simulation, the heat source consists of a volumic heat source of  $50 \text{ W/mm}^3$  extending over a cylindric volume of radius 1.5 mm, plus a Gaussian

surfacic heat source of  $15 \text{ W/mm}^2$  extending over a circular surface of radius 2.5 mm. The values of the convective and radiative heat transfer coefficients are  $H_c = 25 \text{ W/(m}^2\text{C)}$  and  $H_r(T) = \varepsilon\sigma(T^2 + T_{ext}^2)(T + T_{ext})$  where  $\varepsilon = 0.8$ . Again, these transfer coefficients are artificially slightly increased on the lower face in order to account for the cooling effect due to the support.

In the 3D simulations, the maximum temperature reached is  $1760^\circ\text{C}$  on the upper face and  $740^\circ\text{C}$  on the lower face. The computed through-the-thickness temperature distribution is almost identical for both 3D simulations with quadratic and linear elements (Figure 13), and also for the adaptative 3D/shell and local/global approaches (not shown in Figure 13). On the other hand, the through-the-thickness temperature distribution obtained in the simulation using only shell elements is rather inaccurate, the temperature difference between the faces of the shell amounting only to  $410^\circ\text{C}$  versus  $1020^\circ\text{C}$  in the other simulations. This is due to the assumption of quadratic distribution of temperature, which other simulations clearly show to be inadequate in this case (see Figure 13).

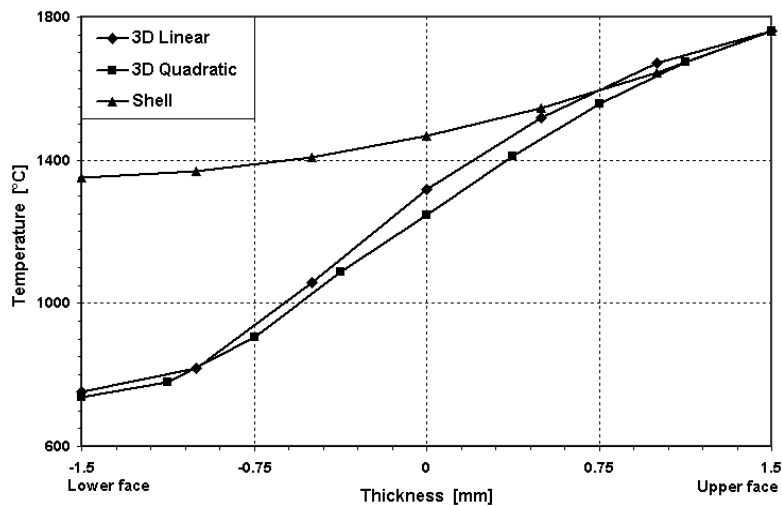


**Figure 13.** *Through-the-thickness distribution of temperature*

All simulations predict that the region near the heat source is entirely transformed into austenite upon heating, then into martensite upon cooling. The metallurgical structure of the rest of the plate remains unaffected.

In the mechanical computation, again, all material properties except Poisson's ratio are considered as temperature- and phase-dependent, transformation plasticity is accounted for and strain hardening is assumed to be of isotropic type.

The adaptative 3D/shell method has not yet been tested for this example. Other methods yield quite good results with regard to residual stresses and strains in the HAZ. We focus here on far residual distortions. Figure 14 shows contours of iso in-plane displacements. All 3 methods tested yield qualitatively similar results. The results of the shell simulation are rather accurate for the lateral displacement, the maximum error made with respect to the reference 3D simulation amounting to 8%. However, this error amounts to 20% for the longitudinal displacement. The local/global simulation yields somewhat less accurate results, the error made on both components of the in-plane displacement being of the order of 20%. (Note that the left portion of the geometry is omitted in the figure because it corresponds to the WME).

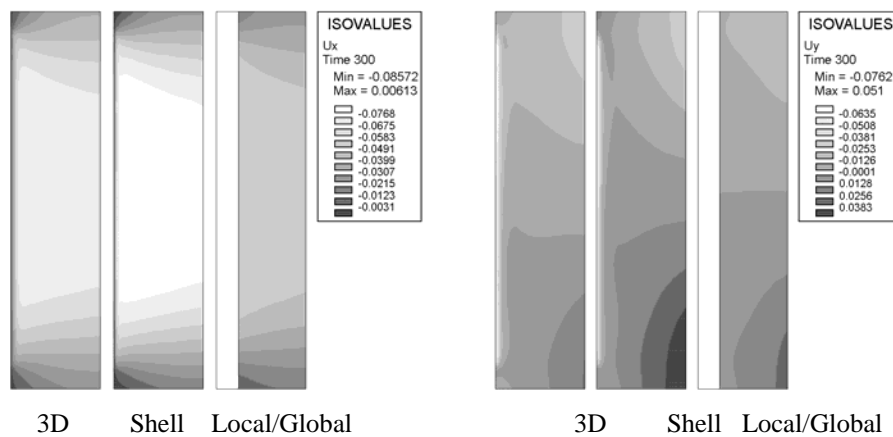


**Figure 14.** Final lateral and longitudinal displacements

Figure 15 shows contours of iso vertical displacement. The results of the shell simulation are not too bad, considering the error made on the through-the thickness temperature gradient. The explanation is tied to the fact that again, the vertical displacement is essentially governed by thermal buckling, as will be detailed below; thus it is more sensitive to the mean temperature in the thickness than to the temperature gradient, and the mean temperature is of course better predicted than the temperature gradient in the shell simulation. The error made by the local/global approach essentially arises from the small displacement hypothesis, which is inadequate to deal with buckling.

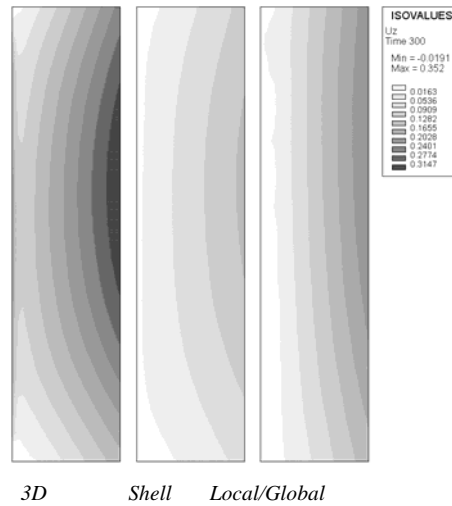


**Figure 15.** Vertical displacement

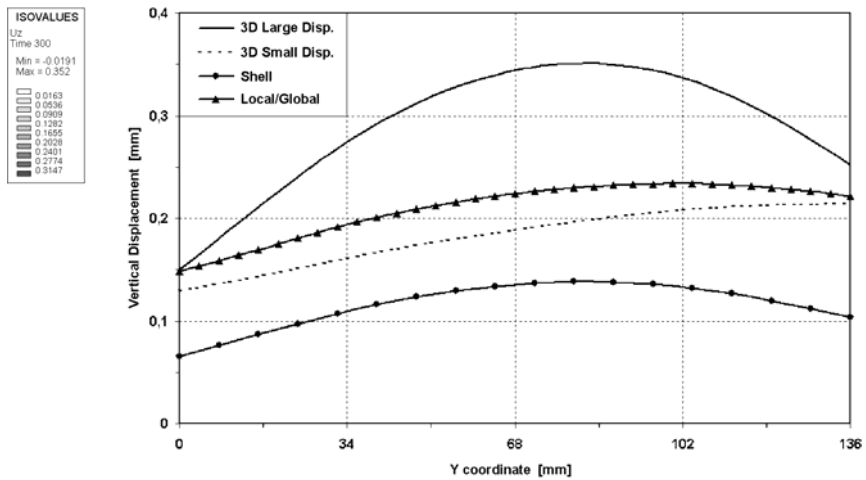


**Figure 16.** Vertical displacement along the length side

Finally Figure 16 shows the distribution of the vertical displacement along the lateral edge of the plate, for all 3 simulations plus an additional 3D one performed with a small displacement hypothesis. The results of this last simulation are quite bad, as compared to those of the 3D simulation fully accounting for large displacements. This substantiates the statement made above that the vertical

displacement is again governed by geometrical nonlinearities arising from thermal buckling.

This example illustrates the capabilities and limits of the new methods proposed to predict distortions of large welded structures. The advantages of these methods are the limited size and relatively short CPU times of the simulations. This is illustrated in Table 1.

	<b>3D</b>	<b>Shell</b>	<b>Local/Global</b>
<b>Number of nodes</b>	12963	1826	8624 <sup>2</sup>
<b>Number of elements</b>	4424	1734	9576 <sup>2</sup>
<b>Thermal analysis</b> <sup>1</sup>	4 h 44 min	1 h 07 min	44 min <sup>2</sup>
<b>Mechanical analysis</b> <sup>1</sup>	7 d 2 h	1 d 1 h 05min	14 h 59 min <sup>2</sup>
<b>Total time</b> <sup>1</sup>	7 d 6 h 44 min	1 d 2 h 12 min	15 h 54 min <sup>3</sup>
<i>1 Computed on a PC 800 MHz, 512 Mo, iterative solver</i>			
<i>2 Local model only</i>			
<i>3 The global system is computed in 11 min.</i>			

**Table 1.** Size and CPU times of the simulations

The advantages of simulations using only shell elements are particularly obvious in this table. (Of course, CPU time, accuracy and memory required depend on the number of layers in the metallurgical and mechanical computations). Also, such simulations can account for effects due to large displacements. The key point consists of adequate calibration of the thermal computation; in order to correctly capture thermal and metallurgical phenomena, as functions of position within the thickness, one should adjust the heat input and/or the heat transfer coefficients so as to get a correct temperature gradient through the thickness. (This has not been done here).

The local/global approach is computationally faster but 2 meshes are required. Also, adequate choice of boundary conditions, in both the thermal and mechanical local simulations, can be problematic since these conditions must incorporate the effect of the rest of the structure in some way.

## 7. Conclusion

Three methods have been presented to predict residual distortions of large thin structures due to welding. Simulations using only shell elements are well fit to some cases. Their main drawback is the assumption of quadratic temperature within the thickness. They are also unfit for such geometries as T-joints. The adaptative 3D/shell approach using a moving local 3D block within some general shell mesh

has been developed to circumvent such problems and seems especially promising. The local/global approach can be used to simulate all types of welding but the geometry of the bead must be simple enough for the size of the local simulation to remain reasonable. Also, it is prone to difficulties with regard to adequate choice of boundary conditions.

The capabilities of these 3 methods have been illustrated in the case of welding of a thin plate. In spite of its apparent simplicity, this problem involves complex material behavior (transformation plasticity) and geometrical nonlinearities. In view of these difficulties, the errors made (as estimated through comparison with some reference fully 3D simulation) can be considered as acceptable.

## 8. References

- Annual Book of ASTM Standard, 1991.
- Bergheau J.M., Vincent Y., Leblond J.B., Jullien J.F., “Viscoplastic behavior of steels during welding”, To appear in *Science and Technology of Welding and Joining*, 2004.
- Dong Y., Hong J.K., Tsai C.L., Dong P., “Finite element modeling of residual stresses in austenitic stainless steel pipe girth welds”, *Welding Journal*, Vol. 76, p. 442s-449s, 1997.
- Greenwood G.W., Johnson R. H., “The deformation of metal under small stresses during phase transformation”, *Proceedings of the Royal Society*, Vol. A 283, p. 403-422, 1965.
- Gu M., Goldak J. A., “Mixing thermal shell and brick elements in FEA of welds”. Proceedings of *OMAE 1991 Conference*, Vol. III-A, *Materials Engineering*, ASME, 1991.
- Hughes T.J.R., Tezduyar T.E., “Finite elements based upon Mindlin plate theory with particular reference to the four-node bilinear isoparametric element”, *ASME Journal of Applied Mechanics*, Vol. 48, p. 587-596, 1981.
- Leblond J.B., Devaux J., “A new kinetic model for anisothermal metallurgical transformations in steels including effect of austenite grain size”, *Acta Metallurgica*, Vol. 32, p. 137-146, 1984.
- Leblond J.B., Devaux J., Devaux J.C., “Mathematical modelling of transformation plasticity in steels. I. Case of ideal-plastic phases”, *International Journal of Plasticity*, Vol. 5, p. 551-572, 1989.
- Leblond J.B., “Mathematical modelling of transformation plasticity in steels. II. Coupling with strain hardening phenomena”, *International Journal of Plasticity*, Vol. 5, p. 573-591, 1989.
- Lindgren L.E., “Modelling for residual stresses and deformations due to welding – ‘Knowing what is not necessary to know’”, *Mathematical Modelling of Weld Phenomena*, Vol. 6, p. 491-518, 2002.
- Lindgren L.E., Karlsson L., “Deformations and stresses in welding of shell structures”, *International Journal for Numerical methods in Engineering*, Vol. 25, p. 635-655, 1988.

- Magee C.L., Transformation kinetics, microplasticity and aging of martensite in Fe-31 Ni, Ph.D. Thesis, Carnegie Institute of Technology, Pittsburgh, USA, 1966.
- Nasstrom M., Wikander L., Karlson L., Lindgren L.E., "Combined 3-D and shell modelling of welding", *Mechanical effects of welding – IUTAM Symposium*, p. 197-206, Lulea, Sweden, 1991.
- Rubin M.B., "Heat conduction in plates and shells with emphasis on a conical shell", *International Journal of Solids and Structures*, Vol. 22, p. 527-551, 1986.
- Souloumiac B., Boitout F., Bergheau J.M., "A new local-global approach for the modelling of welded with steel component distortions", *Mathematical Modelling of Weld Phenomena*, Vol. 6, p. 573-590, 2002.
- Surana K.S., Abusaleh G., "Curved shell elements for heat conduction with p-approximation in the shell thickness direction", *Computers and Structures*, Vol. 34, p. 861-880, 1990.
- Surana K.S., Phillips R. K., "Three dimensional curved shell finite elements for heat conduction", *Computers and Structures*, Vol. 25, p. 775-785, 1987.
- SYSWELD 2002, User's Manual, Engineering Systems International.
- Vincent Y., Simulation numérique des conséquences métallurgiques et mécaniques induites par une opération de soudage – Acier 16MND5, Ph.D. Thesis, INSA Lyon, 2002.
- Vincent Y., Bergheau J.M., Leblond J.B., "Viscoplastic behaviour of steels during phase transformations", *Comptes-Rendus Mécanique*, Vol. 331, p. 587-594, 2003.
- Voltaire F., Andrieux S., « Modèle de thermique pour les coques minces », *Code Aster*, Version 2.6, p. 1-46, 1993.
- Waeckel F., Une loi de comportement thermo-métallurgique des aciers pour le calcul mécanique des structures, Ph.D. Thesis, ENSAM, Paris, France, 1994.